PAPER

Check for updates

BaCu₂Mᴵⱽ Q₄ (Mᴵⱽ = Si, Ge, and Sn; Q = S, Se): synthesis, crystal structures, optical performances and theoretical calculations†

Leyan Nian, [ab] Junben Huang, [b] Kui Wu, *[b] Zhi Su, *[a] Zhihua Yang [iD] [b] and Shilie Pan [iD] *[ab]

Five non-centrosymmetric (NCS) quaternary metal chalcogenides, BaCu₂SiSe₄, BaCu₂GeS₄, BaCu₂GeSe₄, BaCu₂SnS₄, and BaCu₂SnSe₄, were successfully synthesized by solid-state reaction in vacuum-sealed silica tubes. They crystallized in the three different space groups: Ama2 for BaCu₂SnSe₄, P3₁21 for BaCu₂GeS₄ and BaCu₂GeSe₄, and P3₂21 for BaCu₂SiSe₄ and BaCu₂SnS₄. Note that BaCu₂GeS₄ and BaCu₂GeSe₄ show the mirror symmetrical structures to those of BaCu₂SiSe₄ and BaCu₂SnS₄. In comparison with their structures, it can be found that the [CuSe₄] units are connected together to form a two-dimensional (2D) layer structure in BaCu₂SnSe₄, which is different from the 3D framework structure formed by the interlinked [CuQ₄] (Q = S and Se) units in other four title compounds. In addition, BaCu₂SnSe₄ exhibits only one type of tunnel structure with the isolated [BaSe₈] units existing in each tunnel, which is also different from the other title compounds (two types of tunnels with the isolated [BaSe₈] units and [BaSe₆]ₙ chains located). The interesting structural changes also indicate that slight change of cation size would result in different structure features, and future structure prediction should devote considerable attention to the different chalcogen atoms. Moreover, important optical properties (optical bandgap, infrared (IR) absorption edge, second harmonic generation (SHG) response) of the title compounds were systematically investigated. Among them, IR and Raman spectra indicate that all of them exhibit the wide IR absorption edges (~22 μm). Powder SHG measurement shows that BaCu₂SnS₄ possesses good SHG response about 1.6 times that of benchmark AgGaS₂ (AGS) at the particle size 55–88 μm. All results indicate that BaCu₂SnS₄ can be expected as a potential IR nonlinear optical (NLO) candidate. Theoretical calculation was also used to analyze the structure–property relationship and their electronic structures and origin of NLO effect were studied in detail.

Introduction

Frequency-conversion technology on nonlinear optical (NLO) materials was invented to extend the laser wavelength ranges and has been further developed for decades.[1–4] Recently, a series of excellent nonlinear optical (NLO) materials have been

[a]College of Chemistry and Chemical Engineering, Xinjiang Normal University, Urumqi, Xinjiang 830054, China

[b]Key Laboratory of Functional Materials and Devices for Special Environments of CAS, Xinjiang Key Laboratory of Electronic Information Materials and Devices, Xinjiang Technical Institute of Physics & Chemistry of CAS, 40-1 South Beijing Road, Urumqi 830011, China. E-mail: slpan@ms.xjb.ac.cn

† Electronic supplementary information (ESI) available: CIF file; checkcif; atomic coordinates, isotropic displacement parameters; selected bond lengths and angles; powder XRD patterns and IR spectra; particle size versus SHG intensity for BaCu₂SnS₄ and AgGaS₂; absorption spectra of title compounds; calculated electronic structures; projected density of states; calculated SHG density. CCDC 1540053, 1540054, 1540055, 1540056 and 1540057 for BaCu₂SiSe₄, BaCu₂GeS₄, BaCu₂GeSe₄, BaCu₂SnS₄ and BaCu₂SnSe₄, respectively. For ESI and crystallographic data in CIF or other electronic format see DOI: 10.1039/c7ra05022d

discovered and have basically satisfied the demand for the ultraviolet (UV < 400 nm) region.[5–14] However, commercially available IR NLO materials are limited in the IR region because of their inherent performance defects.[15–19] Exploration of new IR NLO materials with outstanding performances is still a challenge to be resolved. During the last few decades, metal chalcogenides have become the preferred investigation system owing to their structural diversities and fascinating physico-chemical properties.[20–33] Most of them contain the tetrahedral units, which have been verified as the "active units" to produce the main contribution for the NLO effect. Note that group 14 elements, such as Si, Ge, and Sn, are generally linked with chalcogens to form the distorted [Mᴵⱽ Q₄] tetrahedra.[34–41] Up to now, a number of new metal chalcogenides with the [Mᴵⱽ Q₄] tetrahedra and attractive NLO performances have been discovered, such as β-K₂Hg₃Ge₂S₈,[36] Li₂CdGeS₄,[42] Na₂BaSnS₄,[43] Na₂-Hg₃Ge₂S₈.[44] The investigation results also indicate that the coordination environments of the cations play a critical role in determining the structures of group 14 elements-containing compounds. Alkaline-earth metals (such as Ba), as high

electropositive elements, have the variable coordination environments with large cation size, so it can affect the structural features and optical properties. In addition, combination of distorted $M^{IV}Q_4$ tetrahedral units and heavy metals into crystal structures may stand a chance to increase the odds of forming acentric structures. Guided by the above-mentioned ideas, we focused our research on the quaternary Ba/Cu/M^{IV}/Q (M^{IV} = Si, Ge, and Sn; Q = S, Se) systems and successfully synthesized five metal chalcogenides, including $BaCu_2SiSe_4$, $BaCu_2GeS_4$, $BaCu_2GeSe_4$, $BaCu_2SnS_4$ and $BaCu_2SnSe_4$. Among them, although the crystal structures of latter four compounds have been previously reported,[45–48] their interesting structural changes and application potential as the IR NLO candidates have not been systematically investigated. Herein, we have studied the structural features and transformation of title compounds and their optical performances (such as optical bandgap, infrared (IR) absorption edge, second harmonic generation (SHG) response) have been reported for the first time. Moreover, theoretical calculation was also used to analyze the structure–property relationship and the origin of NLO effect for title compounds.

Experimental

Reagents and synthesis

All the raw reagents with high purity (4 N) were commercially purchased by Shanghai Aladdin Biochemistry Technology Co., Ltd and used without any further purification. Since the Ba metal is easily oxidized in the air, an Ar-filled glove box was used to avoid the effects of oxygen and moisture in the preparation processes. Conventional high temperature solid-state method was used to synthesize the title compounds.

$BaCu_2GeS_4$ and $BaCu_2SnS_4$

The crystals of $BaCu_2GeS_4$ and $BaCu_2SnS_4$ were synthesized by ratio of the reactants BaS, Cu, Ge/Sn and S in the ratio 1 : 2 : 1 : 3.5. First, the reaction mixture was loaded into the silica tubes (length 20 cm, diameter 10 mm) and sealed with a mixture of methane and oxygen flame under a high vacuum of 10^{-3} Pa. Second, the furnace was programmed by the following steps: heated from room temperature to 600 °C in 30 h and kept at this temperature for 40 h; then, heated to 1050 °C in 20 h and left at this temperature for 100 h; finally, cooled to 400 °C at a rate of 5 °C h^{-1} and then the furnace was shut down to room temperature. Third, the obtained products of title compounds were washed with N,N-dimethylformamide (DMF) to remove the unreacted sulfur and other byproducts. Finally, yellow crystals of $BaCu_2GeS_4$ and red crystals of $BaCu_2SnS_4$ were obtained after drying in air. They are stable in air for several months.

$BaCu_2SiSe_4$, $BaCu_2GeSe_4$, and $BaCu_2SnSe_4$

A stoichiometric mixture of Ba, Cu, M (M = Si, Ge and Sn), and Se in the molar ratio of 1 : 2 : 1 : 4 was loaded into the silica tubes. The increasing temperature-rise program of the three selenides were similar to that of the above two sulfides. The reaction temperature was set to be 1000 °C, which is different

from that for sulfides. After the reaction, the products were also washed by DMF, and many red crystals of $BaCu_2SiSe_4$, $BaCu_2GeSe_4$, and $BaCu_2SnSe_4$ were gained that can be stable in air for several months.

Structure determination

High-quality single crystals were selected by an optical microscope and mounted on glass fibers with epoxy, and then the crystal data was collected on a Bruker SMART APEX II 4K CCD diffractometer with Mo Kα radiation (λ = 0.71073 Å) at 296 K. Lorentz and polarization factors were used to collect the date, and the absorption corrections were completed with multi-scan method.[49] All structure determinations were based on direct method and refined through the full-matrix least-squares on F^2 by SHELXTL crystallographic program package.[50] The final structures were checked with PLATON program,[49] and no other higher symmetries elements were found. Crystallographic data and refinements of the title compounds were summarized in Table 1. The isotropic displacement parameters and atomic coordinates, as well as the results of the bond valence sum (BVS) calculations are given in Table S1 in the ESI.† The bond angles and selected bond distances are shown in Table S2 in the ESI.†

Powder X-ray diffraction

All the compounds were ground to micro-crystals for the powder XRD measurement. The PXRD data were collected on a Bruker D2 X-ray diffractometer equipped with a diffracted beam monochromator set for Cu Kα radiation (λ = 1.5418 Å) at room temperature. The 2θ range was 10–70° with a step size of 0.02° and a fixed counting time of 1 s per step. Seen from Fig. S1 in the ESI,† it can be found that no obvious byproducts was observed and the experimental powder XRD patterns of title compounds are in agreement with the calculated ones derived from the single-crystal data.

UV-vis-near IR diffuse-reflectance and IR spectroscopy

The diffuse-reflectance spectra of title compounds were collected by a Shimadzu SolidSpec-3700DUV spectrophotometer in the wavelength range of 190–2600 nm at room temperature. Then the reflectance spectra were converted to absorption spectra with the Kubelka–Munk function.[51] In addition, IR spectra were also measured with a Shimadzu IR Affinity-1 Fourier transform infrared spectrometer in wavenumber range from 450 to 4000 cm^{-1} using picked single-crystals mixed with KBr pellets.

Raman spectroscopy

The Raman spectra of the crushed crystals of title compounds were collected on a LABRAM HR Evolution spectrometer equipped with a CCD detector using 532 nm radiation from a diode laser. For each sample, crystals were simply placed on a small glass slide and a 50× objective lens was used to choose the area of the crystal specimens to be measured. The grating was set to be 600 gr per mm. The maximum power of 60 mW

Table 1 Crystal data and structure refinement for title compounds

Empirical formula	$BaCu_2GeS_4$	$BaCu_2GeSe_4$	$BaCu_2SiSe_4$	$BaCu_2SnS_4$	$BaCu_2SnSe_4$
f_w	465.25	652.85	608.35	511.35	698.95
Crystal system	Trigonal	Trigonal	Trigonal	Trigonal	Orthorhombic
Space group	$P3_121$	$P3_121$	$P3_221$	$P3_221$	$Ama2$
a (Å)	6.2092(8)	6.5014(6)	6.4188(19)	6.353(3)	11.101(10)
b (Å)	6.2092(8)	6.5014(6)	6.4188(19)	6.353(3)	11.189(10)
c (Å)	15.520(4)	16.266(3)	16.083(10)	15.788(14)	6.728(6)
Z, V (Å^3)	3, 518.20(19)	3, 595.42(16)	3, 573.9(5)	3, 551.8(6)	4, 835.7(13)
D_c (g cm^{-3})	4.473	5.462	5.281	4.616	5.555
μ (mm^{-1})	17.089	32.160	29.673	15.358	29.945
GOF on F^2	1.031	1.054	0.920	0.876	1.018
R_1, wR_2 $(I > 2\sigma(I))^a$	0.0185, 0.0366	0.0281, 0.0659	0.0264, 0.0437	0.0258, 0.0569	0.0251, 0.0527
R_1, wR_2 (all data)^a	0.0214, 0.0373	0.0287, 0.0663	0.0310, 0.0449	0.0317, 0.0594	0.0265, 0.0532
Absolute structure parameter	0.05(3)	0.09(4)	0.07(4)	−0.04(5)	0.06(3)
Largest diff. peak and hole (e Å^{-3})	1.306, −1.117	1.135, −1.207	0.846, −0.809	0.831, −0.945	1.041, −1.691

^{a} $R_1 = F_o − F_c/F_o$ and w$R_2 = [w(F_o{}^2 − F_c{}^2)^2/wF_o{}^4]^{1/2}$ for $F_o{}^2 > 2\sigma(F_o{}^2)$.

and beam diameter of 35 μm were used. The spectrum was collected using an integration time of 5 s.

Second-harmonic generation measurement

By the Kurtz and Perry method,[52] powder SHG responses of title compounds were investigated by a Q-switch Ho:Tm:Cr:YAG laser (2.09 μm, 3 Hz, 50 ns). Polycrystalline samples of the title compounds were ground and sieved into distinct size ranges (0–38, 38–55, 55–88, 88–105, 105–155, 155–200, and 200–250 μm). Then, the samples were pressed between two glass slides in 1 mm thick and secured by a 1 mm thick silicone insole with an 8 mm diameter hole. In the end, they were placed into a light-tight box and irradiated by a pulsed infrared beam and measured with the detector. Oscilloscope was used to record the intensity of the frequency-doubled output emitted from the samples.

Theoretical calculation

Through density functional theory (DFT) calculations tests, we investigated the electronic structures, total and partial density of states (T/PDOS) and optical properties of $BaCu_2M^{IV}Q_4$ (M^{IV} = Si, Ge, and Sn; Q = S, Se). The *ab initio* DFT method calculations were performed by the plane wave pseudopotential implemented in the CASTEP package.[53] The local density approximations (LDA) with CA–PZ functional,[54,55] a 900 eV cutoff energy for the plane-wave basis set and norm-conserving pseudopotentials (NCP)[56] was employed in all computations. The Brillouin zone was integrated using Monkhorst–Pack-generated sets of k-points and we determined $3 \times 3 \times 2$ k-point meshes for the former four target compounds and a $4 \times 4 \times 2$ for $BaCu_2SnSe_4$. The configurations for diverse electron orbital generating pseudopotentials were Ba $5p^6$ $6s^2$, Cu $3p^6$ $3d^{10}$ $4s^1$, Si $3s^2$ $3p^2$, Ge $4s^2$ $4p^2$, Sn $5s^2$ $5p^2$, S $3s^2$ $3p^4$ and Se $4s^2$ $4p^4$ and the other calculating parameters used in the calculations and convergent criteria were set by the default values of the CASTEP code. To explore the contributions from different structural units to the NLO coefficients, the SHG density method was performed by using the effective SHG: Virtual-Electron (VE) and Virtual-Hole

(VH).[2] At a zero frequency, the formula of second-order NLO coefficients can be derived as[57]

$$\chi^{\alpha\beta\gamma} = \chi^{\alpha\beta\gamma}(\text{VE}) + \chi^{\alpha\beta\gamma}(\text{VH}) \quad (1)$$

where,

$$\chi^{\alpha\beta\gamma}(\text{VH}) = \frac{e^3}{2\hbar^2 m^3} \sum_{vv'c} \int \frac{d^3k}{4\pi^3} P(\alpha\beta\gamma) \text{Im} \left[p_{vv'}{}^\alpha p_{v'c}{}^\beta p_{cv}{}^\gamma \right]$$
$$\times \left(\frac{1}{\omega_{cv}{}^3 \omega_{v'c}{}^2} + \frac{2}{\omega_{vc}{}^4 \omega_{cv'}} \right) \quad (2)$$

$$\chi^{\alpha\beta\gamma}(\text{VE}) = \frac{e^3}{2\hbar^2 m^3} \sum_{vcc'} \int \frac{d^3k}{4\pi^3} P(\alpha\beta\gamma) \text{Im} \left[p_{vc}{}^\alpha p_{cc'}{}^\beta p_{c'v}{}^\gamma \right]$$
$$\times \left(\frac{1}{\omega_{cv}{}^3 \omega_{vc'}{}^2} + \frac{2}{\omega_{vc}{}^4 \omega_{c'v}} \right) \quad (3)$$

here, α, β, γ are Cartesian components, v and v′ denote valence bands, c and c′ denote conduction bands, and $P(\alpha\beta\gamma)$ denotes full permutation. The band energy difference and momentum matrix elements are denoted as $\hbar\omega_{ij}$ and $P_{ij}{}^\alpha$, respectively.

Results and discussion

Crystal structure

Although all title compounds have the similar formula $BaCu_2$-$M^{IV}Q_4$, they crystallize in the different polar space groups. Among them, $BaCu_2SnSe_4$ crystallizes in the $Ama2$ space group of orthorhombic system, whereas other four compounds crystallize in the trigonal system. In other words, while through the simple element substitution (Sn to Ge, or Se to S) in $BaCu_2$-$SnSe_4$, they show obvious structural transformation from orthorhombic to trigonal system. Note that $BaCu_2GeS_4$ and $BaCu_2GeSe_4$ crystallize in the $P3_121$ space group, while $BaCu_2$-$SiSe_4$ and $BaCu_2SnS_4$ crystallize in the mirror symmetry $P3_221$ space group. The current crystal date is consistent with the previously reported phases.[45–48]

BaCu$_2$SiSe$_4$

It crystallizes in a polar trigonal space group $P3_221$ with $Z = 3$ and its asymmetric unit consists of one Ba, one Cu, one Si, two Se atoms. It exhibits a 3D framework structure built up of isolated [SiSe$_4$] tetrahedra and edge or corner-sharing linked [CuSe$_4$] ligands with charge-balanced Ba cations located at the framework tunnels (Fig. 1a). The isolated [SiSe$_4$] ligands are approximately regular tetrahedra with d(Si–Se) = 2.263(2) to 2.269(2) Å, which is comparable to those of other known seleno-silicates.[58,59] The distorted [CuSe$_4$] units with d(Cu–Se) = 2.428(5) to 2.539(1) Å link together by sharing corners and edges to form the 3D tunnel structure. Note that two types (type I and type II) of tunnels that formed with the interconnection of the [CuSe$_4$] units are interestingly found, such as six-member ring (6-MR) and 4-MR (Fig. 2a). In addition, the [BaSe$_8$] polyhedra only locate within the 6-MR tunnels and show two types of connection modes: (i) exist in the isolation (Fig. 2b); (ii) link with each other by sharing Se corners to form the isolated [BaSe$_6$]$_n$ chains (Fig. 2c). Each [BaSe$_8$] unit is linked with eight other [BaSe$_8$] units by sharing corners and edges in the b–c plane. Then, the [BaSe$_8$] ligands in the different tunnels still interlink by sharing corners and edges to make up framework structure.

BaCu$_2$GeSe$_4$

It crystallizes in the trigonal $P3_121$ space group that shows the mirror symmetry compared with the structure of BaCu$_2$SiSe$_4$.
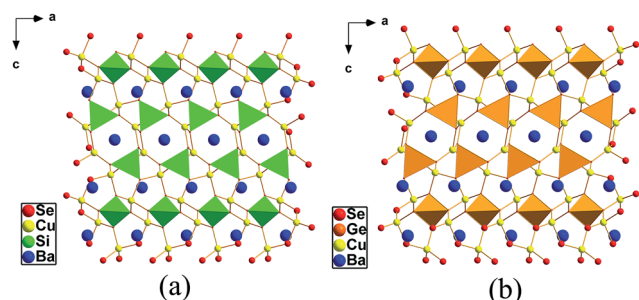

Fig. 1 (a) Crystal structure of BaCu$_2$SiSe$_4$; (b) crystal structure of BaCu$_2$GeSe$_4$.
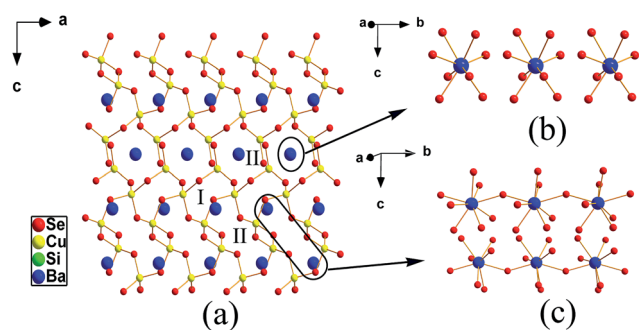

Fig. 2 (a) Two different types of tunnels (I and II) that formed with the interconnection of the [CuSe$_4$] units in BaCu$_2$SiSe$_4$ and the Ba atoms only exist in the tunnel II; (b) [BaSe$_8$] polyhedra exist in the isolation in the tunnel II; (c) isolated [BaSe$_6$]$_n$ chains in the tunnel II.

Seen from its structure, the [CuSe$_4$] units with d(Cu–Se) = 2.427(1) to 2.541(2) Å link with isolated [GeSe$_4$] units with d(Ge–Se) = 2.352(16) to 2.361(15) Å to form two types of 3D tunnel structure (6-MR and 4-MR), which is similar with the structural features in BaCu$_2$SiSe$_4$. In addition, the existence patterns of [BaSe$_8$] polyhedra in BaCu$_2$GeSe$_4$ are in consistence with that in BaCu$_2$SiSe$_4$. Note that the arrangement direction of [GeSe$_4$] units in BaCu$_2$GeSe$_4$ is opposite with that in the BaCu$_2$SiSe$_4$, thus, it show mirror symmetry structure with that of BaCu$_2$SiSe$_4$.

BaCu$_2$SnSe$_4$

It crystallizes in a polar orthorhombic space group $Ama2$ with $Z = 4$ and one crystallographically unique Ba, one Sn, one Cu, three Se atoms locate in its asymmetric unit. Seen from its structure (Fig. 3a), the irregular [CuSe$_4$] with d(Cu–Se) = 2.431(3) to 2.546(2) Å are firstly linked with each other by sharing corners and edges to form the layer structure in the ac plane (Fig. 3b). Then, isolated [SnSe$_4$] tetrahedra with d(Sn–Se) = 2.509(3)–2.545(2) Å as further bridge with these layers form the 3D tunnel structure along the c-axis, which may generate a wide range of applications for this compound, such as conductive material, heat-transfer material, ionic absorption, and photocatalysis.[60–62] The Ba atoms exist inside the tunnels and are linked with eight Se atoms showing d(Ba–Se) range from 3.311(2) to 3.409(2) Å to form distorted [BaSe$_8$] polyhedra, which is close to those of other related compounds, including BaGa$_4$Se$_7$ (3.429–3.861 Å)[21] and Ba$_7$Sn$_3$Se$_{13}$ (3.183–3.761 Å).[63] Each [BaSe$_8$] unit is linked with six other [BaSe$_8$] units by sharing corners and edges in the b–c plane. Note that the [BaSe$_8$] polyhedra exist isolated in the same tunnel (Fig. 3c), but the [BaSe$_8$] polyhedra in the different tunnels connect together by
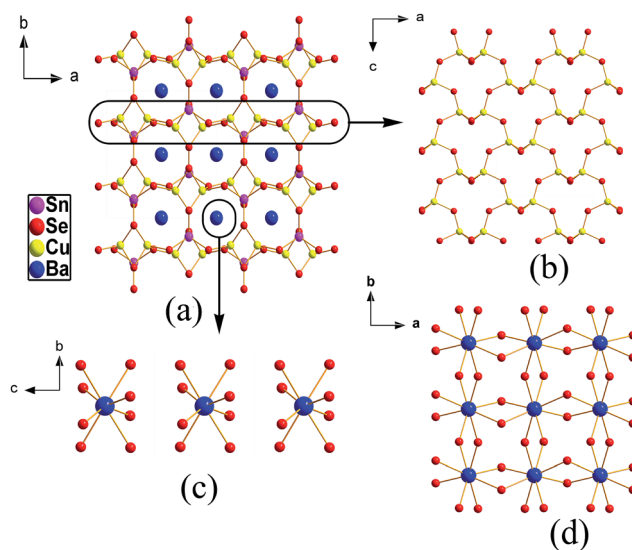

Fig. 3 (a) Crystal structure of BaCu$_2$SnSe$_4$; (b) regular [CuSe$_4$] units are linked with each other to form the layer structure in the ac plane; (c) isolated [BaSe$_8$] polyhedra exist in the same tunnel; (d) [BaSe$_8$] polyhedra by sharing corners and edges to make up framework structure.

sharing corners and edges to make up framework structure (Fig. 3d).

Structural comparison

In view of their similar structures among the four compounds ($BaCu_2SiSe_4$, $BaCu_2GeS_4$, $BaCu_2GeSe_4$, $BaCu_2SnS_4$), we have chosen the $BaCu_2SiSe_4$ and $BaCu_2SnSe_4$ as the representatives to discuss their structural comparison and the results can be extended to all of title compounds. In comparison with the structures of $BaCu_2SiSe_4$ and $BaCu_2SnSe_4$, they have some similarities: all of them have the $[BaSe_8]$ octahedra and isolated $[M^{IV}Se_4]$ (M^{IV} = Si and Sn) tetrahedra in their structures. However, they still have several obviously different features in their structures: (i) the asymmetric unit and Z (number of molecules in a unit cell) of $BaCu_2SiSe_4$ have five crystallographically distinct sites and $Z = 3$, which are different from those of $BaCu_2SnSe_4$ (6 and $Z = 4$); (ii) the $[BaSe_8]$ units are more highly distorted in $BaCu_2SnSe_4$ than those in $BaCu_2SiSe_4$, owing to the largest difference (Δd) between Ba–Se that Δd (Ba–Se) = 0.098 Å in $BaCu_2SnSe_4$ is larger than that (0.066 Å) in $BaCu_2SiSe_4$; (iii) the $[CuSe_4]$ units link together to make up the tunnel structure in $BaCu_2SiSe_4$, whereas the $[CuSe_4]$ units connect with each other to form layer structure in $BaCu_2SnSe_4$; (iv) note that the $[BaSe_8]$ polyhedra exist in isolation in each tunnel of $BaCu_2SnSe_4$, but in $BaCu_2SiSe_4$, the $[BaSe_8]$ polyhedra show two types of connection modes: isolation and chain; (v) each $[BaSe_8]$ unit is linked with six other $[BaSe_8]$ units in $BaCu_2SnSe_4$, which is different from that each $[BaSe_8]$ polyhedron connects with eight other $[BaSe_8]$ units in $BaCu_2SiSe_4$. Similarly, the main structural differences as mentioned above are also found between $BaCu_2SnSe_4$ and other compounds. Interestingly, previous researches show that the structures of metal chalcogenides can be changed with the different M or Q atoms in crystal structures.[44] Therefore, this observation indicates that the slight change of cation size would result in different structure features, and future structure prediction should be devoted considerable attentions to the different chalcogen atoms (Fig. 4).

Optical properties

The diffuse-reflectance UV-vis-NIR spectra of title compounds (Fig. S3 in the ESI†) were measured, and the spectral results show that the experimental band gaps are 2.62 eV for
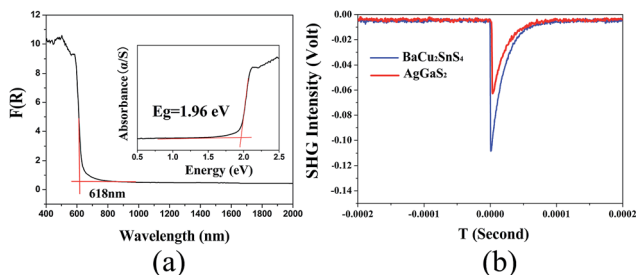
$BaCu_2SiSe_4$, 2.47 eV for $BaCu_2GeS_4$, 1.88 eV for $BaCu_2GeSe_4$, 1.96 eV for $BaCu_2SnS_4$ and 1.72 eV for $BaCu_2SnSe_4$, respectively. Among them, $BaCu_2SiSe_4$ and $BaCu_2GeS_4$ have larger band gaps, which are comparable to those of commercial AGS (2.64 eV). The other three compounds have relatively narrow band gaps that are still comparable to those of other typical IR NLO crystals, such as $ZnGeP_2$ (1.65 eV) and $AgGaSe_2$ (1.75 eV). IR spectra of title compounds were also measured on the microcrystal powders, and the results (Fig. S2 in the ESI†) reveal that all of them have wide transmission regions from 4000–450 cm^{-1}, namely, 2.5–22 μm, that cover the two important atmospheric transparent windows of 3–5 and 8–12 μm, which are comparable to the IR absorption edges of other IR NLO powdered compounds such as $BaGa_4Se_7$ (~18 μm),[21] $LiCdGeS_4$ (~22 μm),[35] AGS (~23 μm),[64] $SnGa_4S_7$ (~25 μm),[65] $Li_4HgGe_2S_7$ (~22 μm)[66] and $CsCd_4Ga_5S_{12}$ (~25 μm).[23] Raman spectra (Fig. 5) also further verify that title compounds have the wide IR transmission region and no absorption peaks in the region of 450–1000 cm^{-1} (10–22 μm). As for the selenides, the obvious absorption peaks include $BaCu_2SiSe_4$ (221.5 cm^{-1}), $BaCu_2GeSe_4$ (275 cm^{-1}) and $BaCu_2SnSe_4$ (195 cm^{-1}), which can be assigned to the characteristic absorptions of the Si–Se, Ge–Se, and Sn–Se modes, respectively. As for the sulfides, the absorption peaks for $BaCu_2GeS_4$ and $BaCu_2SnS_4$ are 367.5 and 337.5 cm^{-1} that correspond to the Ge–S and Sn–S bonding interactions, respectively. The intensive peak positions for the family of $BaCu_2M^{IV}Q_4$ are affected by the tetravalent (IV) metals, and the peak positions slightly shifted towards the short wavelength with the change of the M^{IV} cations (from Si to Sn).[44] By comparing the absorption peaks of sulphides ($BaCu_2GeS_4$ and $BaCu_2SnS_4$) and selenides ($BaCu_2SiSe_4$, $BaCu_2GeSe_4$ and $BaCu_2SnSe_4$), the peak positions shifted towards the short wavelength when the anion Q vary from S to Se. SHG responses for title compounds were also systemically measured with a 2.09 μm Q-switch laser in different particle sizes at room temperature and commercial AGS crystal was used as a reference. Among them, $BaCu_2SnS_4$ has a good SHG response that is about

Fig. 4 (a) Experimental band gap of $BaCu_2SnS_4$; (b) SHG intensities of $BaCu_2SnS_4$ *versus* $AgGaS_2$ at the particle size of 55–88 μm.

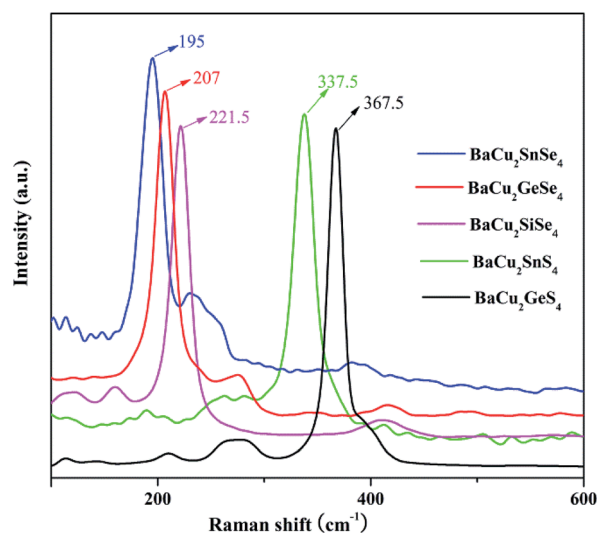**Fig. 5** Raman spectra of title compounds.

1.6 times that of benchmark AGS in the particle size range 55–88 μm (Fig. S4 in the ESI†) and the other four compounds show the weak SHG responses about 0.3 times of AGS in the particle size range 55–88 μm. Note that SHG intensities were decreased with the increase of particle sizes for all of title compounds, which indicates that they exhibit the non-phase matching behavior.

Theoretical studies

First-principles computations were adopted to better understand the electronic structures of the title compounds. Based on the theoretical electronic structures (Fig. S5 in the ESI†), the highest point of the valence band (VB) and the lowest point of the conduction band (CB) locate at the different points for $BaCu_2SnSe_4$, which indicates that it is an indirect band gap compound, whereas the other four compounds are direct band gap semiconductors. Calculated results show that the theoretical band gaps are 1.53 eV for $BaCu_2GeS_4$, 1.31 eV for $BaCu_2GeSe_4$, 1.63 eV for $BaCu_2SiSe_4$, 1.09 eV for $BaCu_2SnS_4$ and 1.07 eV for $BaCu_2SnSe_4$ (Fig. 6a for $BaCu_2SnS_4$, Fig. S5† for other compounds, respectively), respectively. The calculated band gaps are lower than the experimental values, which can be attributed to the discontinuity of exchange–correlation energy of the GGA functional.[67,68] Moreover, the PDOS of title compounds were also obtained (Fig. S6 in the ESI†). From the PDOS of $BaCu_2SnS_4$ (Fig. 6b), the region in the valence bands from -8 eV to Fermi level is mainly occupied by Cu-3d and S-3p states. Meanwhile, the bottom of conduction bands is derived from the S-3p and Sn-5s orbitals. As for the other four compounds, their T/PDOS were also achieved and familiar with that of $BaCu_2SnS_4$. Moreover, SHG coefficients (d_{ij}) for title compounds were also calculated. Since $BaCu_2SiSe_4$, $BaCu_2GeS_4$, $BaCu_2GeSe_4$ and $BaCu_2SnS_4$ belong to 32 point group that allows for five nonzero coefficients in the SHG tensor and only two are independent: $d_{11} = -d_{12} = -d_{26}$ and $d_{14} = -d_{25}$. However, the allowed coefficients from five to three were reduced by Kleinman symmetry,[69] and results the condition that

$d_{14} = -d_{25} = 0$, so the four compounds only have one independent NLO tensor (d_{11}). The theoretical SHG coefficients (d_{ij}) are $d_{11} = 0.28$ pm V^{-1} for $BaCu_2GeS_4$, $d_{11} = 5.62$ pm V^{-1} for $BaCu_2GeSe_4$, $d_{11} = 4.18$ pm V^{-1} for $BaCu_2SiSe_4$, and $d_{11} = 12.09$ pm V^{-1} for $BaCu_2SnS_4$, respectively. In addition, $BaCu_2SnSe_4$ belongs to $mm2$ group that has three unequal NLO coefficients: $d_{31} = 1.76$, $d_{32} = -12.65$ and $d_{33} = -10.13$ pm V^{-1}. In comparison with their calculated SHG coefficients (d_{ij}) values, it can be found that $BaCu_2GeS_4$, $BaCu_2GeSe_4$, and $BaCu_2SiSe_4$ are smaller than that of $BaCu_2SnS_4$, which are also consistent with their experimental results. Unfortunately, the SHG experimental observation ($0.3\times$ AgGaS$_2$) is smaller than that ($d_{32} = -12.65$ pm V^{-1}) of $BaCu_2SnSe_4$, which may be by its narrow optical bandgap (1.72 eV) and long shortwave absorption edge (up to 1 μm). Thus, the SHG light (1045 nm) was likely to be weaken under the fundamental light (2090 nm), and then lead to the low SHG intensity. We believe that the precise SHG effect may be obtained by the long wavelength laser (e.g. carbon dioxide laser) for $BaCu_2SnSe_4$. Note that $BaCu_2SnS_4$ exhibits a comparable SHG coefficient (12.09 pm V^{-1}) to that of commercial AGS (11 pm V^{-1}). Meanwhile, SHG density method was also used to investigate the origin of SHG responses for title compounds. The contributions of VE and VH to the total SHG coefficients were obtained using the band-resolved method, and the results were listed in Table S3 in the ESI.† As for $BaCu_2SnS_4$, the VH and VE contributions were about 90.01% (d_{11}) and 9.99% (d_{11}), respectively. Therefore, we chose the occupied and unoccupied of VH to investigate the mainly origin of the SHG response for $BaCu_2SnS_4$. Fig. 6c and d plot the occupied and unoccupied states of VH and clearly showing that the SHG effect of $BaCu_2SnS_4$ was derived from the [CuS$_4$] and [SnS$_4$] tetrahedra. In addition, the contributions of VE and VH for other four compounds were similar to that of $BaCu_2SnS_4$ (Fig. S7 in the ESI†), which indicate that their origins of SHG effects are mainly derived from the cooperative contribution of the [CuQ$_4$] and [MQ$_4$] units.

Conclusions

In summary, a family of NCS quaternary $BaCu_2M^{IV}Q_4$ (M^{IV} = Si, Ge, and Sn; Q = S, Se) were successfully synthesized and characterized. Interestingly, title compounds crystallize in different space groups. Among them, $BaCu_2GeS_4$ and $BaCu_2GeSe_4$ crystallize in the trigonal space group $P3_121$ that are mirror symmetric with $BaCu_2SiSe_4$ and $BaCu_2SnS_4$ (space group $P3_221$), while $BaCu_2SnSe_4$ crystallizes in the orthorhombic space group $Ama2$. In $BaCu_2SnSe_4$, irregular [CuSe$_4$] units are firstly linked with each other by sharing corners and edges to form a 2D layer structure in the ac plane, and then the isolated [SnSe$_4$] tetrahedra as a bridge connect with these layers to form a 3D tunnel structure along the c-axis. Different from the structure that all the [BaSe$_8$] units of $BaCu_2SnSe_4$ existed in the same tunnel structure in isolation in $BaCu_2SnSe_4$, other four title compounds exhibit two types of tunnel structure (I, 4-MR and II, 6-MR) with the isolated [BaSe$_8$] units and [BaSe$_6$]$_n$ chains existed in the tunnel II. Raman and IR spectra indicate that their IR absorption edges can reach to 22 μm, which covers the two
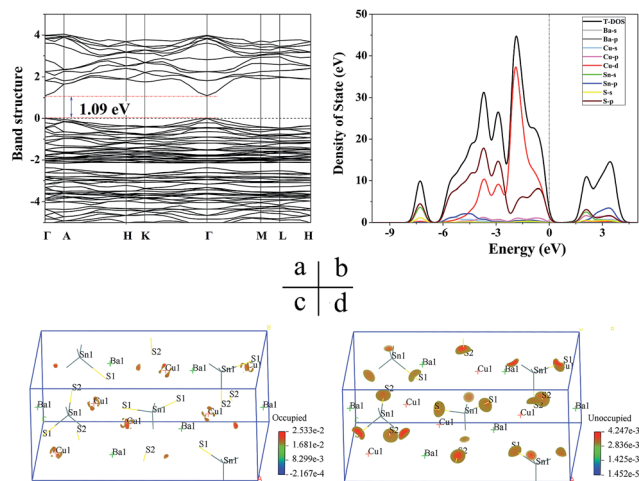

Fig. 6 (a) Calculated band gap of $BaCu_2SnS_4$; (b) PDOS of $BaCu_2SnS_4$; (c) SHG-density of $BaCu_2SnS_4$ at VH occupied; (d) SHG-density of $BaCu_2SnS_4$ at VH unoccupied.

critical atmospheric transparent windows (3–5 and 8–14 μm). Experimental band gaps of $BaCu_2SiSe_4$ and $BaCu_2GeS_4$ are 2.47 and 2.62 eV, respectively, and larger than those of other typical materials, which imply that they may exhibit the large LDTs and are applied in the high-power laser system. In addition, the results of SHG measurements indicate that $BaCu_2SnS_4$ has a good SHG response about 1.6 times of that AGS in the particle size range 55–88 μm. The overall research results indicate that $BaCu_2SnS_4$ has a promising application as a potential NLO material in the IR region.

Acknowledgements

Notes and references

1 R. J. Seymour and F. Zernike, *Appl. Phys. Lett.*, 1976, **29**, 705.
2 J. Lin, M. H. Lee, Z. P. Liu, C. T. Chen and C. J. Pickard, *Phys. Rev. B: Condens. Matter Mater. Phys.*, 1999, **60**, 13380.
3 C. T. Chen, B. C. Wu, A. D. Jiang and G. M. You, *Sci. China, Ser. B*, 1985, **28**, 235.
4 G. D. Boyd, T. J. Bridges, C. K. N. Patel and E. Buehler, *Appl. Phys. Lett.*, 1972, **21**, 553.
5 T. Q. Sun, P. Shan, H. Chen, X. W. Liu, H. D. Liu, S. L. Chen, Y. A. Cao, Y. F. Kong and J. J. Xu, *CrystEngComm*, 2014, **16**, 10497.
6 T. T. Tran, H. Yu, J. M. Rondinelli, K. R. Poeppelmeier and P. S. Halasyamani, *Chem. Mater.*, 2016, **28**, 5238.
7 S. G. Zhao, P. F. Gong, L. Bai, X. Xu, S. Q. Zhang, Z. H. Sun, Z. S. Lin, M. C. Hong, C. T. Chen and J. H. Luo, *Nat. Commun.*, 2014, **5**, 4019.
8 H. P. Wu, S. L. Pan, K. R. Poeppelmeier, H. Y. Li, D. Z. Jia, Z. H. Chen, X. Y. Fan, Y. Yang, J. M. Rondinelli and H. S. Luo, *J. Am. Chem. Soc.*, 2011, **133**, 7786.
9 H. P. Wu, H. W. Yu, Z. H. Yang, X. L. Hou, X. Su, S. L. Pan, K. R. Poeppelmeier and J. M. Rondinelli, *J. Am. Chem. Soc.*, 2013, **135**, 4215.
10 L. Li, Y. Wang, B. H. Lei, S. J. Han, Z. H. Yang, K. R. Poeppelmeier and S. L. Pan, *J. Am. Chem. Soc.*, 2016, **138**, 9101.
11 H. W. Yu, H. P. Wu, S. L. Pan, Z. H. Yang, X. L. Hou, X. Su, Q. Jing, K. R. Poeppelmeier and J. M. Rondinelli, *J. Am. Chem. Soc.*, 2014, **136**, 1264.
12 S. G. Zhao, P. F. Gong, S. Y. Luo, S. J. Liu, L. N. Li, M. A. Asghar, T. Khan, M. C. Hong, Z. S. Lin and J. H. Luo, *J. Am. Chem. Soc.*, 2015, **137**, 2207.
13 M. Zhang, X. Su, S. L. Pan, Z. Wang, H. Zhang, Z. H. Yang, B. B. Zhang, L. Y. Dong, Y. Wang, F. F. Zhang and Y. Yang, *J. Phys. Chem. C*, 2014, **118**, 11849.
14 H. P. Wu, S. L. Pan, H. W. Yu, D. Z. Jia, A. M. Chang, H. Y. Li, F. F. Zhang and X. Huang, *CrystEngComm*, 2012, **14**, 799.
15 T. X. Zhu, X. G. Chen and J. G. Qin, *Front. Chem. Sci. Eng.*, 2011, **6**, 1.
16 P. F. Bordui and M. M. Fejer, *Annu. Rev. Mater. Sci.*, 1993, **23**, 321.
17 A. Jayaraman, V. Narayanamurti, H. Kasper, M. Chin and R. Maines, *Phys. Rev. B: Solid State*, 1976, **14**, 3516.
18 A. Harasaki and K. Kato, *Jpn. J. Appl. Phys., Part 1*, 1997, **36**, 700.
19 G. Catella, L. Shiozawa, J. Hietanen, R. Eckardt, R. Route, R. Feigelson, D. Cooper and C. Marquardt, *Appl. Opt.*, 1993, **32**, 3948.
20 D. J. Mei, P. F. Gong, Z. S. Lin, K. Feng, J. Y. Yao, F. Q. Huang and Y. C. Wu, *CrystEngComm*, 2014, **16**, 6836.
21 J. Y. Yao, D. J. Mei, L. Bai, Z. S. Lin, W. L. Yin, P. Z. Fu and Y. C. Wu, *Inorg. Chem.*, 2010, **49**, 9212.
22 G. M. Li, K. Wu, Q. Liu, Z. H. Yang and S. L. Pan, *J. Am. Chem. Soc.*, 2016, **138**, 7422.
23 H. Lin, L. J. Zhou and L. Chen, *Chem. Mater.*, 2012, **24**, 3406.
24 H. Lin, L. Chen, J. S. Yu, H. Chen and L. M. Wu, *Chem. Mater.*, 2017, **29**, 499.
25 G. M. Li, Q. Liu, K. Wu, Z. H. Yang and S. L. Pan, *Dalton Trans.*, 2017, **46**, 2778.
26 X. S. Lin, G. Zhang and N. Ye, *Cryst. Growth Des.*, 2009, **9**, 1186.
27 Z. Z. Luo, C. S. Lin, W. L. Zhang, H. Zhang, Z. Z. He and W. D. Cheng, *Chem. Mater.*, 2013, **26**, 1093.
28 S. P. Guo, Y. Chi and G. C. Guo, *Coord. Chem. Rev.*, 2016, **335**, 44.
29 F. Liang, L. Kang, Z. S. Lin and Y. C. Wu, *Cryst. Growth Des.*, 2017, **17**, 2254.
30 Y. Kim, I.-s. Seo, S. W. Martin, J. Baek, P. Shiv Halasyamani, N. Arumugam and H. Steinfink, *Chem. Mater.*, 2008, **20**, 6048.
31 I. Chung, M. G. Kim, J. I. Jang, J. Q. He, J. B. Ketterson and M. G. Kanatzidis, *Angew. Chem., Int. Ed.*, 2011, **50**, 10867.
32 I. Chung and M. G. Kanatzidis, *Chem. Mater.*, 2013, **26**, 849.
33 Z. M. Ma, F. Weng, Q. R. Wang, Q. Tang, G. H. Zhang, C. Zheng, R. P. S. Han and F. Q. Huang, *RSC Adv.*, 2014, **4**, 28937.
34 C. D. Morris, H. Li, H. Jin, C. D. Malliakas, J. A. Peters, P. N. Trikalitis, A. J. Freeman, B. W. Wessels and M. G. Kanatzidis, *Chem. Mater.*, 2013, **25**, 3344.
35 J. A. Brant, D. J. Clark, Y. S. Kim, J. I. Jang, J. H. Zhang and J. A. Aitken, *Chem. Mater.*, 2014, **26**, 3045.
36 J. H. Liao, G. M. Marking, K. F. Hsu, Y. Matsushita, M. D. Ewbank, R. Borwick, P. Cunningham, M. J. Rosker and M. G. Kanatzidis, *J. Am. Chem. Soc.*, 2003, **125**, 9484.
37 K. A. Rosmus, J. A. Brant, S. D. Wisneski, D. J. Clark, Y. S. Kim, J. I. Jang, C. D. Brunetta, J. H. Zhang, M. N. Srnec and J. A. Aitken, *Inorg. Chem.*, 2014, **53**, 7809.
38 N. Zhen, K. Wu, Y. Wang, Q. Li, W. H. Gao, D. W. Hou, Z. H. Yang, H. D. Jiang, Y. J. Dong and S. L. Pan, *Dalton Trans.*, 2016, **45**, 10681.
39 N. Ding, D. Y. Chung and M. G. Kanatzidis, *Chem. Commun.*, 2004, 1170.
40 K. Wu, X. Su, Z. H. Yang and S. L. Pan, *Dalton Trans.*, 2015, **44**, 19856.

41 K. Wu, S. Pan and Z. Yang, *RSC Adv.*, 2015, **5**, 33646.

42 J. W. Lekse, M. A. Moreau, K. L. McNerny, J. Yeon, P. S. Halasyamani and J. A. Aitken, *Inorg. Chem.*, 2009, **48**, 7516.

43 K. Wu, Z. H. Yang and S. L. Pan, *Angew. Chem., Int. Ed.*, 2016, **55**, 6713.

44 K. Wu, Z. H. Yang and S. L. Pan, *Chem. Mater.*, 2016, **28**, 2795.

45 M. Tampier and D. Johrendt, *Z. Anorg. Allg. Chem.*, 2001, **627**, 312.

46 A. Assoud, N. Soheilnia and H. Kleinke, *Chem. Mater.*, 2005, **17**, 2255.

47 C. Teske and O. Vetter, *Z. Anorg. Allg. Chem.*, 1976, **426**, 281.

48 C. Teske, *Z. Naturforsch., B: J. Chem. Sci.*, 1979, **34**, 386.

49 A. Spek, *J. Appl. Crystallogr.*, 2003, **36**, 7.

50 A. Bruker and A. Saint, *Acta Crystallogr., Sect. A: Found. Crystallogr.*, 2008, **64**, 112.

51 P. Kubelka, *Z. Tech. Phys.*, 1931, **12**, 593.

52 S. Kurtz and T. Perry, *J. Appl. Phys.*, 1968, **39**, 3798.

53 S. J. Clark, M. D. Segall, C. J. Pickard, P. J. Hasnip, M. I. Probert, K. Refson and M. C. Payne, *Z. Kristallogr.*, 2005, **220**, 567.

54 J. P. Perdew and A. Zunger, *Phys. Rev. C: Nucl. Phys.*, 1981, **23**, 5048.

55 D. M. Ceperley and B. Alder, *Phys. Rev. Lett.*, 1980, **45**, 566.

56 D. Hamann, M. Schlüter and C. Chiang, *Phys. Rev. Lett.*, 1979, **43**, 1494.

57 B. B. Zhang, M. H. Lee, Z. H. Yang, Q. Jing and S. L. Pan, *Appl. Phys. Lett.*, 2015, **106**, 031906.

58 W. L. Yin, K. Feng, R. He, D. J. Mei, Z. S. Lin, J. Y. Yao and Y. C. Wu, *Dalton Trans.*, 2012, **41**, 5653.

59 Z. Z. Luo, C. S. Lin, H. H. Cui, W. L. Zhang, H. Zhang, H. Chen, Z. Z. He and W. D. Cheng, *Chem. Mater.*, 2015, **27**, 914.

60 J. J. Suk, H. D. Won and L. J. Sung, *Catal. Today*, 2007, **120**, 174.

61 D. Huang, C. Persson, Z. P. Ju, M. F. Dou, C. M. Yao and J. Guo, *Europhys. Lett.*, 2014, **105**, 37007.

62 J. D. Beasley, *Appl. Opt.*, 1994, **33**, 1000.

63 A. Assoud and H. Kleinke, *Chem. Mater.*, 2005, **17**, 4509.

64 A. Okorogu, S. Mirov, W. Lee, D. Crouthamel, N. Jenkins, A. Y. Dergachev, K. Vodopyanov and V. Badikov, *Opt. Commun.*, 1998, **155**, 307.

65 Z. Z. Luo, C. S. Lin, H. H. Cui, W. L. Zhang, H. Zhang, Z. Z. He and W. D. Cheng, *Chem. Mater.*, 2014, **26**, 2743.

66 K. Wu, Z. H. Yang and S. L. Pan, *Chem. Commun.*, 2017, **53**, 3010.

67 L. Sham and M. Schlüter, *Phys. Rev. Lett.*, 1983, **51**, 1888.

68 A. J. Cohen, P. Mori-Sanchez and Y. Weitao, *Phys. Rev. B*, 2008, **77**, 115123.

69 D. Kleinman, *Phys. Rev.*, 1962, **126**, 1977.